Predicting Phase Stability at Interfaces

J. Pitfield®,* N. T. Taylor®, and S. P. Hepplestone®†
University of Exeter, Stocker Road, Exeter EX4 4QL, United Kingdom

We present the RAFFLE methodology for structural prediction of the interface between two materials and demonstrate its effectiveness by applying it to MgO encapsulated by two layers of graphene. To address the challenge of interface structure prediction, our methodology combines physical insights derived from morphological features observed in related systems with an iterative machine learning technique. This employs physical-based methods, including void-filling and n-body distribution functions to predict interface structures. For the carbon-MgO encapsulated system, we have shown the rocksalt and hexagonal phases of MgO to be the two most energetically stable in the few-layer regime. We demonstrate that monolayer rocksalt is heavily stabilized by interfacing with graphene, becoming more energetically favorable than the graphenelike monolayer hexagonal MgO. The RAFFLE methodology provides valuable insights into interface behavior, and a route to finding new materials at interfaces.

New materials can form at the interface between two others due to the unique strains and bonding environments at play [1,2]. These *interface materials* can significantly affect the behavior of the overall system and, as such, there is an ever-growing interest in exploring their potential for device applications. The impact of interface materials covers many aspects, including electrical [3–6] and thermal [7–11] conductivity, mechanical strength [12–14], and other unique properties [15–17]. Interfaces in devices can be tailored by choice of growth technique, which influences the interface stoichiometry [18,19], defects [20–22], strains [23–25], constituent surfaces [26–28], and many other factors. Their ability to improve device performance has been studied for solar cells [29–33], batteries [34–37], and other electronic devices [38–40]. All this makes interface materials a promising avenue for materials design and engineering.

The wealth of unusual and unique properties predicted and observed at interfaces are due to a combination of the vast quantity of possible configurations, and the unusual local bonding environment. Many other interactions are at play at interfaces, including strains, induced electric and magnetic fields and unconventional stoichiometries, and as such, characterizing and fabricating specific interfaces is nontrivial [41–43]. Hence, theoretical structural prediction is key. Structure prediction has gone through many evolutions, from coincident site lattice approaches [44–48],

to random structure searches [49–52], genetic algorithms [53–56], machine learning [57–60], and species swapping explorations [61]. The prediction of interface structures introduces new challenges to this paradigm [62], with increased constraints and variation along with higher computational cost and lower availability of reference data.

Interfaces, and hence interface materials, can be formed in several different ways, including intercalation [63] and encapsulation. These present a more accessible form of interface structure to explore. Recently, both monolayer metal oxides [64] and halides [65] have been fabricated between graphene sheets. Monolayer monoxides have been suggested to occur in a different phase from that of their respective bulks [66,67]. Interestingly, the structure adopted is often a graphenelike hexagonal phase, as in the case of MgO [68]. However, experimental evidence provided by Vasu *et al.* [69] offers the possibility of another form of monolayer MgO in these interfaces.

For bulk MgO, the rocksalt (RS) cubic phase is the theoretical [70–73] and experimental [74–77] ground state, with hexagonal phase MgO (h-MgO) theorized as a metastable step within the phase transition of wurtzite (WZ) to RS. The WZ phase is found to be unstable in bulk [70,78], although it is the ground state configuration of some metal oxides [79–83], and a metastable phase in others [84–86]. The h-MgO phase has a larger volume per formula unit than the RS phase, necessitating a negative pressure to realize priority formation of the h-MgO over the RS. In the encapsulated case, the thinnest regions of MgO have indicated, via transmission electron microscopy (TEM) imaging [69], a mixture of a monolayer rocksaltlike phase, and other hexagonal-like regions. Differing MgO phases can be formed by various routes [87–93]. including alloying [70], forming low-dimensional structures

(i.e., nanotubes) [92], or strains resulting from interface formation [93].

In this report, we outline a method to predicting the structure of interface materials, with a focus on its application to MgO confined—or *encapsulated*—in graphene: RAFFLE (PseudoRandom Approach For Finding Local Energetic minima). This allows us to search for phases of MgO at the interface between sheets of graphene, identify those phases that appear in experiment, and postulate as to the nature of those unidentified. We then explore these phases in more detail, varying the number of layers and strain to obtain insight into their formation. To this end, we present the RAFFLE structural prediction method for interfaces.

An interface consists of two *surfaces* close together, with an *interface region* located between the two bulks, as indicated in Fig. 1(a). To model the interface structure, we have developed a strategy combining machine learning, empirical potentials, and physical intuition. First, we identify the materials that constitute the interface—in this case graphene and MgO. We then (i) populate atomic species-dependent distribution functions from databases of known materials and structures [94–108] and (ii) generate a series of supercells containing the two host materials, and a suitably sized vacuum region, the interface region, separating them. This *region* is filled with atoms using a variety of probability functions derived from the distribution functions. The resultant structures are then relaxed and the energetics calculated. These are then ranked by their formation energy and used to evolve the distribution

functions, which define atomic placement for the next set of structures to be generated. Termination of this process follows some heuristic criteria: (i) the lowest energy structure is recaptured multiple times [109] and (ii) observation(s) of hybrid phases consisting of mixtures of those repeated ground states.

Key to this approach is the placement of atoms in the interface region which are informed by distribution functions. Any method that employs machine learning within the context of materials science must use (a set of) metrics that obey symmetry invariance. To achieve this, uniform descriptors are represented in a spatially invariant form so as to remove the issue of representing the geometry of equivalent systems in multiple forms. The first general function employed here is the spherically invariant bond length distribution function, which highlights the frequency of neighbors as a function of distance, i.e., bond lengths. The second distribution describes the radially invariant angle between two bond pairs of a common atom. Finally, a four-body or plane-angle distribution function is introduced as the angle between an atom and a plane formed from three others, which has the translational invariance required for generalization. These three (probabilistic) distribution functions are physically appealing as the two-body is used to characterize amorphous structures [110,111], the three-body is inspired by the Keating potential [112], and the four-body is a dihedral angle fluctuation [113]; and all these have been applied in neural networks [114]. These functions can be interchanged, or extended beyond four-body, allowing for adaptation as necessary. As the search progresses, previously generated structures are used to update the distribution functions. Fig. 1(c) shows the two-body distribution evolution as subsequent structures are included. These interatomic distribution functions are explored here as both characterization functions, and as functions designed to aid in the inverse design of energetically favorable interface structures. Further details are given in the Supplemental Material [115].

Having developed the descriptors of the atomic environment, the next step is to build sensible host unit cells with an interface region for the structure search, as depicted in Fig. 1. Interface structure search differs from bulk structure search in that the host cell is constrained by the two adjacent materials, which imposes several factors that must be considered in order to form an appropriate supercell: (i) to reduce the strain between the two host materials, the mismatch between their corresponding lattice vectors should be minimized; (ii) the thickness of each surrounding host material should ideally reach its bulk limit; (iii) the interface region needs to be appropriately thick; (iv) the supercell ideally needs to be small enough to be feasible within theoretical energetic evaluation; (v) supercells with different underlying Bravais lattices need to be created, to avoid creating false interface materials. These constraints create both limitations and
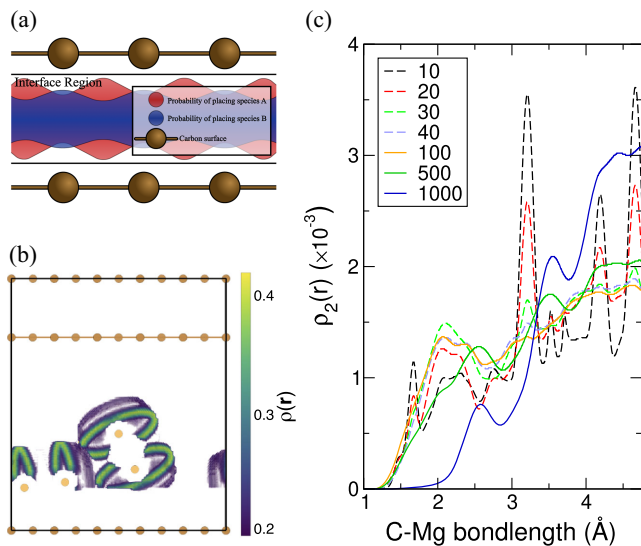

FIG. 1. (a) Illustration demonstrating the concept of the RAFFLE methodology at interfaces, with calculated probabilities of placement for species of atoms present within the interface region. (b) Heatmap of the probability surface of placing the subsequent Mg atom within the graphene-graphene interface according to the (combined *n*-body) distribution functions. (c) The two-body distribution function between Mg and C atoms, evolving from the first 10 structures considered to 1000.

compromises on any interface structure search. Methods and tools already exist to generate supercells for interfaces, such as ARTEMIS [150], which is used here.

Having set up the species-dependent placement probability functions and the host structure, we now generate the interface material. This involves evaluating the host structure and identifying the most suitable sites. The RAFFLE method combines three different approaches, which focus on different aspects such as thoroughness and completeness, computational cost, and entropic maximization. The three methods are (1) a full grid search, (2) a pseudorandom walk, and (3) a void-finding method.

In the first placement method—the *full grid search* method—the full space of the supercell is discretized into a grid. At each point, a test atom is postulated, and the suitability of this atom to be placed is queried according to the placement functions. For all of the points considered, that with the highest degree of probability is selected as the most viable site and an atom is randomly inserted near that position.

The second placement method—the *pseudorandom* method—involves selecting a random point within the unit cell and determining its suitability for accommodating a test atom, where this probability is assessed using the aforementioned placement functions, using a probabilistic pass/fail criteria; a pass is achieved if the probability from the placement function is above a defined threshold. If the check fails, nearby points are randomly sampled for improvements, and if a point is found to be better then the process is repeated. In this manner, a form of pseudorandom walk is conducted until a suitable spot is found or the number of failed steps exceeds a tolerance (typically 10 000 fails). A net failure to place repeats the procedure, selecting a new random point and initializing a new random walk, until a suitable pseudorandom point can be selected.

The final placement method is the *void-finding* method which follows the same basis outlined for the full grid search method, but instead of evaluating n-body distribution functions, the emptiest region of the search space is located and an atom is randomly inserted near that position. The frequency of this call dictates the uniformity of the interface region as well as providing seeds for further random walks, ultimately filling out empty regions quickly.

For each test atom, one of the three placement methods is randomly selected, where the likelihood of each is guided by an adjustable ratio. If one function is successful then an atom is placed. If it fails, then a different approach is selected. This procedure allows us to generate a variety of interface structures, with probabilistic nature of the search enabling new structures each time. The combination of the void function (which seeds empty spaces) and the pseudorandom method of placement around existing atoms allows us to fill large supercells rapidly.

The rules developed for RAFFLE provide our physical insight into the system, allowing for the system to learn over generations and evolve. As structures are generated, evaluated, and relaxed, each is used to update the form of the distribution functions using a suitable weighting function (see Supplemental Material [115]). We emphasize that the probabilistic nature of our approach means that theoretically all configurations will be searched, while the evolution procedure provides a bias towards successful features and speeds up the search.

Application of the RAFFLE approach to C-MgO systems begins with noting that the surfaces present in this case are both graphene, providing a clean match between two single cells of graphene. From these, cubic, monoclinic, and hexagonal supercells are generated to provide the base for interface structure searching. Some of the most relevant supercells employed are presented in Fig. S7 [115].

Fig. 1(c) depicts the evolution of the two-body (interatomic distance) distribution between magnesium and carbon as a function of the number of structures explored. Early iteration structures suggest that structures with C-Mg separations of 3.1 Å are most favorable, yet this peak disappears as more structures are analyzed. A new peak appears at 3.25 Å, which corresponds to the interlayer separation identified in the most stable structures for encapsulated MgO found in this Letter. As the n-body distribution functions are combined to form a three-dimensional probability map for placement of new ions, we can visualize this as a probability map across the cell, as shown in Fig. 1(b). The rings depicted are a result of the probability function accurately mapping a combination of the n-body distribution functions, with the radius of these rings corresponding to an optimum interatomic separation (two-body contribution), and the orientation of multiple rings an indication of both the 90° and 120° bond angle found in RS and h-MgO, respectively (three-body contribution). The probability placement function localizes around ions, leaving voids of empty space within the cell. This empty space is mapped by the void finding approach, depicted in Fig. S4 [115], showing that a combination of these two methods allows placement across the cell.

Through analysis of the generated structures we obtain the key quantities of $E_{\text{interface}}$ and E_{surface}, which are the interface and surface formation energies, respectively, defined in the usual manner and given in Section SIV A [115].

The results of the structure search for the C-MgO system are presented in Fig. 2. All structures are presented with respect to the most energetically favorable found structure. Structures identified are shown in Fig. 2(a) and the most stable are highlighted in the Fig. 2(b). These highlight the two most stable phases, where the encapsulated form of RS-MgO is the most stable, followed by h-MgO.

C-MgO has been previously suggested to possess a square lattice of single- to few-layer thickness [69], alongside other regions which clearly contain noncubic lattices or polycrystalline regions. We find evidence to support that
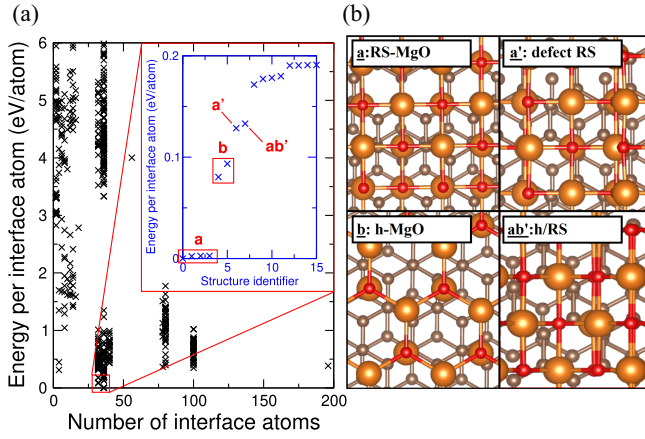
(a) (b)

FIG. 2. Energy per interface atom for (a) all structures considered and (inset) the 16 most stable interface structures as identified, during the C-MgO RAFFLE search. (b) Structures of low-energy systems.

(a) (b)

FIG. 3. (a) Formation energy versus volume for bulk and graphene-encapsulated four-layer RS- and h-MgO (encapsulated energies are shifted by the corresponding interface). Black dashed lines denote common tangent constructions. Green (red) shaded regions highlight the increase in volume range—from bulk to encapsulated—spanned by the constructions for RS-MgO (h-MgO). (b) Formation energies of the surface and interface for RS- and h-MgO for varying MgO thicknesses. RS- and h-MgO formation energies are most comparable for thicknesses in the range of 4–6.5 Å (inserts depict dominant phases).

the WZ phase is not stabilized by encapsulation within graphene; the phase is absent from Fig. 2 entirely, and encapsulated structures generated matching this phase reconfigure during relaxation from the WZ to the h-MgO phase. The phase change curve of isolated MgO from WZ to h-MgO involves no activation energy, hence, geometric optimization finding no local minima agrees with previous investigations in bulk [70].

Our structure search reveals the most stable family of structures in Fig. 2 is the RS-MgO phase encapsulated within graphene. This is in line with cubic structure(s) seen in regions of TEM [69] images of the fabricated encapsulated MgO. The RS phase of MgO is also the only strong candidate from the orthonormal family of phases (cubic, tetragonal, etc.) which matches with the experimental observations of Vasu *et al.* Interfacial RS-MgO has the lowest formation energy of the considered interface structures, in parity with bulk RS-MgO occupying the ground state.

The next most stable phase our search reveals is h-MgO, with fivefold coordinated inplane bonding with the graphenelike structure aligned parallel to the graphene sheets (shown in out Fig. S6 [115]). We note a $0.05|e|/$atom decrease in magnitude of average charge from RS to the h phase, which corresponds to weaker bonding due to an average increase in bond lengths of 0.06 Å. This expansion, and the cubic (sixfold) RS bonding compared to the hexagonal (fivefold) h-MgO bonding, is highlighted by Fig. 3(a), with h-MgO corresponding to a volume increase per formula unit of 4.5 Å^3. As the formation energies of interfacial RS and h-MgO are within 0.1 eV/atom of each other, both phases are explored to a greater depth to identify the likely specifics of the interface composition.

Comparison of the minima of energy-volume curves for different material phases can provide insight into their relative stabilities. Here, we report a value of 0.14 eV/pair
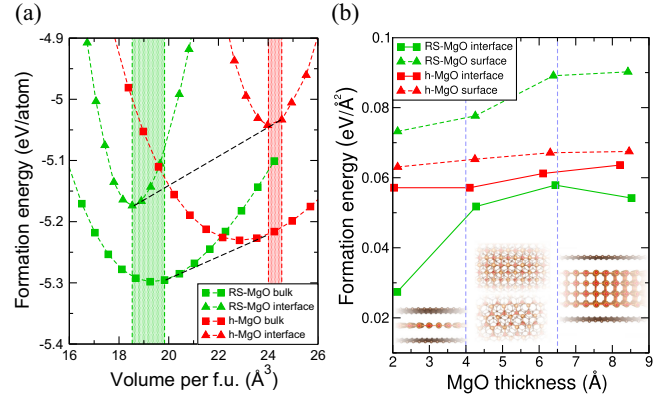
between the RS and h-phase bulks, in agreement with the Materials Project [101] value of 0.175 eV/pair. In Fig. 3(a) the bulk and interface structures of both RS and h-MgO are strained and the formation energies are shown as a function of the volume per interface atom. The figure demonstrates that the h-MgO (RS) phase is more favorable in the highly strained (compressed) regime. The energy separation of the RS and h-MgO minima in the interface system is calculated at 0.26 eV/formula unit, increasing the energy gap between the phases to 0.12 eV/formula unit compared to bulk. In comparison to the volume per formula unit profile of bulk, the h-MgO in encapsulation is higher in formation energy by 0.38 eV/formula unit. Similarly, the formation energy of the RS phase is increased by 0.24 eV/formula unit. For the interface, two-phase mixtures of RS and h-MgO become more energetically viable than a single phase. This is due to the greater difference in energetic minima for interfaces (as a function of volume per formula unit) compared to the bulks.

A key difference between the RS-MgO and h-MgO structures depicted in Fig. 2 is the number of layers present. We consider the variation with layers of the interface energy, as depicted in Fig. 3(b), and identify three key regions. The first is the monolayer region, in which the RS-like monolayer interfaced with graphene displays a difference of 0.05 eV/Å^3. This indicates that formation of an interface between RS-MgO and graphene massively stabilizes monolayer RS-MgO. The significance of this result shows a difference between supported (i.e., placed on a substrate) and encapsulated systems. Previous works [68,151] have indicated h-MgO as the more favorable phase for supported monolayer MgO, whereas our results

show instead that full encapsulation enables the formation of monolayer RS-MgO. The second region of 2–3 layers thickness (4–6.5 Å) is notable for the energy difference between the RS and h-MgO phases, which is less than $0.005 \text{ eV}/\text{Å}^3$. This small energy difference presents the thickness for which two phase mixtures have the smallest difference in energy, up to the four layers considered. The final region of 4+ layers thickness (6.5 + Å) shows the surface energy for the RS and h-MgO diverging as the RS-MgO decreases in energy and h-MgO increases. In this thicker region, two phase mixtures are less favorable. Overall, we observe that both phases show reduction in the formation energy due to the passivation provided by encapsulation. However, this effect is much greater for the RS phase than the h phase as the RS-MgO surface formation energy is much higher than h-MgO. Thus the RS phase gains more from encapsulation due to charge transfer than the h phase. Hence encapsulated structures tend to have more favorable RS interfaces whereas exposed surfaces will prefer h-MgO [68,151].

Mixtures of the RS and h-MgO appear higher in energy than either constituent phase, notably the ab' hybrid phase, as shown in Fig. 2. The magnitude of this energy difference is, however, only 0.05 eV/atom from h-MgO, indicating the existence of potential polycrystalline phases. The hexagonal bonding is found to be out of plane with the graphene, and causes significant distortion in the graphene layers, which corresponds to both a higher overall energy and indicates the existence of more stable hybrid phases. The formation of these hybrid phase mixtures of RS and h-MgO compensates for strains at the interface, as suggested by both Figs. 3(a) and 3(b). This prediction is consistent with Vasu $et\ al.$, in which their TEM identifies both cubic and hexagonal regions. Our results clearly suggest that the RS phase remains the most stable even in the nanoencapsulated form. Fig. 3(b) shows that the monolayer RS MgO is more stable when interfaced with graphene than the isolated surface, supporting that monolayer RS MgO has been fabricated. However, the stability of h-MgO is within 0.1 eV/atom, and less than $0.01 \text{ eV}/\text{Å}^2$ [Fig. 3(b)], of the cubic phase at thicknesses between 2–3 layers. This suggests the phase of MgO exhibited in noncubic regions of the TEM is in fact a fabrication of h-MgO, rather than the wurtzite phase.

Here, we have presented the RAFFLE methodology for structural prediction of interface materials. RAFFLE employs physical-based methods, such as void-filling (the raising of entropy), and n-body distribution functions (homogeneity and isotropy) to predict interface structures ranked via formation energies. The distribution functions evolve within the structural search, and thus act as identifiers for stability and inverse design descriptors for structural generation. This approach provides a method for finding new materials at interfaces. We have demonstrated this by applying RAFFLE to study the previously fabricated system of MgO encapsulated between layers of graphene, showing few-layer form of MgO to be the rocksalt and hexagonal phases. We demonstrate that monolayer RS is heavily stabilized by interfacing with graphene, having its surface energy reduced by 0.4 eV/atom compared to the isolated surface, becoming more energetically favorable than the graphenelike monolayer h-MgO. This presents an avenue for the fabrication of polar monolayers which have previously proved elusive [152,153]. Other phases present in the RAFFLE search that exist close in formation energy to the RS and h-MgO are identified as combinations of those structures, including rotations and defects, further confirming our identification of the lowest energy structures in the C-MgO landscape. Our results open up the exciting possibility of exploring further interface structures and finding new materials in these regimes.

*joepitfield@gmail.com
†S.P.Hepplestone@exeter.ac.uk

[1] C. Hill, R. Beach, and T. McGill, J. Vac. Sci. Technol. B **18**, 2044 (2000).

[2] R. Oxland, S. W. Chang, X. Li, S. W. Wang, G. Radhakrishnan, W. Priyantha, M. J. H. van Dal, C. H. Hsieh, G. Vellianitis, G. Doornbos, K. Bhuwalka, B. Duriez, I. Thayne, R. Droopad, M. Passlack, C. H. Diaz, and Y. C. Sun, IEEE Electron Device Lett. **33**, 501 (2012).

[3] S. Zhang, A. Hao, N. Nguyen, A. Oluwalowo, Z. Liu, Y. Dessureault, J. G. Park, and R. Liang, Carbon **144**, 628 (2019).

[4] T. J. Marks, Angew. Chem., Int. Ed. Engl. **29**, 857 (1990).

[5] T. Ma, H.-L. Gao, H.-P. Cong, H.-B. Yao, L. Wu, Z.-Y. Yu, S.-M. Chen, and S.-H. Yu, Adv. Mater. **30**, 1706435 (2018).

[6] G. Schusteritsch, S. P. Hepplestone, and C. J. Pickard, Phys. Rev. B **92**, 054105 (2015).

[7] G. Chen, J. Heat Transfer **119**, 220 (1997).

[8] C.-W. Nan, G. Liu, Y. Lin, and M. Li, Appl. Phys. Lett. **85**, 3549 (2004).

[9] N. Burger, A. Laachachi, M. Ferriol, M. Lutz, V. Toniazzo, and D. Ruch, Prog. Polymer Sci. **61**, 1 (2016).

[10] Q. Liu, F. Wang, W. Shen, X. Qiu, Z. He, Q. Zhang, and Z. Xie, Ceram. Int. **45**, 23815 (2019).

[11] P. Lv, X.-W. Tan, K.-H. Yu, R.-L. Zheng, J.-J. Zheng, and W. Wei, Carbon **99**, 222 (2016).

[12] C. Yi, X. Chen, F. Gou, C. M. Dmuchowski, A. Sharma, C. Park, and C. Ke, Carbon **125**, 93 (2017).

[13] H. Gong, Mater. Chem. Phys. **126**, 284 (2011).

[14] X. Chen, L. Zhang, C. Park, C. C. Fay, X. Wang, and C. Ke, Appl. Phys. Lett. **107**, 253105 (2015).

[15] G. Tuttle, H. Kroemer, and J. H. English, J. Appl. Phys. **67**, 3032 (1990).

[16] P. Yu, Y.-H. Chu, and R. Ramesh, Mater. Today **15**, 320 (2012).

[17] H. Pinto, R. Jones, J. P. Goss, and P. R. Briddon, Phys. Rev. B **82**, 125407 (2010).

[18] N. T. Taylor, F. H. Davies, S. G. Davies, C. J. Price, and S. P. Hepplestone, Adv. Mater. **31**, 1904746 (2019).

[19] C. Malerba, F. Biccari, C. L. A. Ricardo, M. Valentini, R. Chierchia, M. Müller, A. Santoni, E. Esposito, P. Mangiapane, P. Scardi *et al.*, J. Alloys Compd. **582**, 528 (2014).

[20] J. Gubicza, *Defect Structure and Properties of Nanomaterials* (Woodhead Publishing, Cambridge, 2017).

[21] S. McDonnell, R. Addou, C. Buie, R. M. Wallace, and C. L. Hinkle, ACS Nano **8**, 2880 (2014).

[22] J. Zhang, J. Shi, D.-C. Qi, L. Chen, and K. H. Zhang, APL Mater. **8**, 020906 (2020).

[23] V. M. Kaganer, B. Jenichen, F. Schippan, W. Braun, L. Däweritz, and K. H. Ploog, Phys. Rev. Lett. **85**, 341 (2000).

[24] S. Demirci, H. H. Gürel, S. Jahangirov, and S. Ciraci, Nanoscale **12**, 3249 (2020).

[25] V. M. Kaganer, B. Jenichen, F. Schippan, W. Braun, L. Däweritz, and K. H. Ploog, Phys. Rev. B **66**, 045305 (2002).

[26] R. Del Sole, J. Phys. C **8**, 2971 (1975).

[27] R. Del Sole and G. Onida, Phys. Rev. B **60**, 5523 (1999).

[28] W. Sun, V. Dierolf, and H. Jain, Phys. Status Solidi (b) **258**, 2000427 (2021).

[29] H. Zhou, Q. Chen, G. Li, S. Luo, T.-b. Song, H.-S. Duan, Z. Hong, J. You, Y. Liu, and Y. Yang, Science **345**, 542 (2014).

[30] A. A. Sutanto, N. Drigo, V. I. Queloz, I. Garcia-Benito, A. R. Kirmani, L. J. Richter, P. A. Schouwink, K. T. Cho, S. Paek, M. K. Nazeeruddin *et al.*, J. Mater. Chem. A **8**, 2343 (2020).

[31] S. Chen, J. R. Manders, S.-W. Tsang, and F. So, J. Mater. Chem. **22**, 24202 (2012).

[32] C. E. Patrick and F. Giustino, Adv. Funct. Mater. **21**, 4663 (2011).

[33] E. Baker, J. Pitfield, C. J. Price, and S. P. Hepplestone, J. Phys. Condens. Matter **34**, 375001 (2022).

[34] C. Yan, H. Yuan, H. S. Park, and J.-Q. Huang, J. Energy Chem. **47**, 217 (2020).

[35] C. J. Price, J. Pitfield, E. Baker, and S. P. Hepplestone, Phys. Chem. Chem. Phys. **25**, 2167 (2023).

[36] L. Xu, S. Tang, Y. Cheng, K. Wang, J. Liang, C. Liu, Y.-C. Cao, F. Wei, and L. Mai, Joule **2**, 1991 (2018).

[37] Y. Xiao, Y. Wang, S.-H. Bo, J. C. Kim, L. J. Miara, and G. Ceder, Nat. Rev. Mater. **5**, 105 (2020).

[38] N. Koch, ChemPhysChem **8**, 1438 (2007).

[39] C. Jia and X. Guo, Chem. Soc. Rev. **42**, 5642 (2013).

[40] K. M. Razeeb, E. Dalton, G. L. W. Cross, and A. J. Robinson, Int. Mater. Rev. **63**, 1 (2018).

[41] J. Chen, J. Feng, B. Xiao, K. Zhang, Y. Du, Z. Hong, and R. Zhou, J. Mater. Sci. Technol. (Sofia) **26**, 49 (2010).

[42] D. Jiang, J. Long, M. Cai, Y. Lin, P. Fan, H. Zhang, and M. Zhong, Mater. Des. **114**, 185 (2017).

[43] M. Tabuchi, R. Takahashi, M. Araki, K. Hirayama, N. Futakuchi, Y. Shimogaki, Y. Nakano, and Y. Takeda, Appl. Surf. Sci. **159**, 250 (2000).

[44] L. Jelver, P. M. Larsen, D. Stradi, K. Stokbro, and K. W. Jacobsen, Phys. Rev. B **96**, 085306 (2017).

[45] F. Therrien, P. Graf, and V. Stevanović, J. Chem. Phys. **152**, 074106 (2020).

[46] A. Zur and T. McGill, J. Appl. Phys. **55**, 378 (1984).

[47] L. Yang, L. Huang, Y. Yao, and L. Jiao, Appl. Catal., B **282**, 119584 (2021).

[48] S. Y. Ren and J. D. Dow, Appl. Phys. Lett. **69**, 251 (1996).

[49] C. J. Pickard and R. Needs, J. Phys. Condens. Matter **23**, 053201 (2011).

[50] J. Chou, C. Hsing, C. Wei, C. Cheng, and C. Chang, J. Phys. Condens. Matter **25**, 125305 (2013).

[51] D. B. Putungan, S.-H. Lin, and J.-L. Kuo, ACS Appl. Mater. Interfaces **8**, 18754 (2016).

[52] A. R. Oganov, C. J. Pickard, Q. Zhu, and R. J. Needs, Nat. Rev. Mater. **4**, 331 (2019).

[53] A. Supady, V. Blum, and C. Baldauf, J. Chem. Inf. Model. **55**, 2338 (2015).

[54] S. M. Woodley, Appl. Evol. Comput. Chem. **110**, 95 (2004).

[55] S. Wu, M. Ji, C.-Z. Wang, M. C. Nguyen, X. Zhao, K. Umemoto, R. Wentzcovitch, and K.-M. Ho, J. Phys. Condens. Matter **26**, 035402 (2013).

[56] Q. Zhu, V. Sharma, A. R. Oganov, and R. Ramprasad, J. Chem. Phys. **141**, 154102 (2014).

[57] M. K. Bisbo and B. Hammer, Phys. Rev. Lett. **124**, 086102 (2020).

[58] E. Musa, F. Doherty, and B. R. Goldsmith, Curr. Opin. Chem. Eng. **35**, 100771 (2022).

[59] Q. Zhu, A. Samanta, B. Li, R. E. Rudd, and T. Frolov, Nat. Commun. **9**, 467 (2018).

[60] B. Meredig, A. Agrawal, S. Kirklin, J. E. Saal, J. W. Doak, A. Thompson, K. Zhang, A. Choudhary, and C. Wolverton, Phys. Rev. B **89**, 094104 (2014).

[61] A. J. Morris, C. P. Grey, and C. J. Pickard, Phys. Rev. B **90**, 054111 (2014).

[62] B. Zhu, G. Schusteritsch, P. Lu, J. L. MacManus-Driscoll, and C. J. Pickard, APL Mater. **7**, 061105 (2019).

[63] J. Zhou, Z. Lin, H. Ren, X. Duan, I. Shakir, Y. Huang, and X. Duan, Adv. Mater. **33**, 2004557 (2021).

[64] A. Dahal and M. Batzill, Sci. Rep. **5**, 1 (2015).

[65] F. Withers, T. H. Bointon, M. F. Craciun, and S. Russo, ACS Nano **7**, 5052 (2013).

[66] B. Luo, B. Yao, E. Tian, H. Song, X. Wang, G. Li, K. Xi, B. Li, H. Song, and L. Li, Proc. Natl. Acad. Sci. U.S.A. **116**, 17213 (2019).

[67] H. Zheng, X.-B. Li, N.-K. Chen, S.-Y. Xie, W. Q. Tian, Y. Chen, H. Xia, S. B. Zhang, and H.-B. Sun, Phys. Rev. B **92**, 115307 (2015).

[68] J. Goniakowski, C. Noguera, and L. Giordano, Phys. Rev. Lett. **93**, 215702 (2004).

[69] K. Vasu, E. Prestat, J. Abraham, J. Dix, R. Kashtiban, J. Beheshtian, J. Sloan, P. Carbone, M. Neek-Amal, S. Haigh *et al.*, Nat. Commun. **7**, 1 (2016).

[70] S. Limpijumnong and W. R. L. Lambrecht, Phys. Rev. B **63**, 104103 (2001).

[71] A. B. Belonoshko, S. Arapan, R. Martonak, and A. Rosengren, Phys. Rev. B **81**, 054110 (2010).

[72] G. Cappellini, F. Finocchi, S. Bouette-Russo, and C. Noguera, Comput. Mater. Sci. **20**, 401 (2001).

[73] A. R. Oganov, M. J. Gillan, and G. D. Price, J. Chem. Phys. **118**, 10174 (2003).

[74] F. Coppari, R. Smith, J. Eggert, J. Wang, J. Rygg, A. Lazicki, J. Hawreliak, G. Collins, and T. Duffy, Nat. Geosci. **6**, 926 (2013).

[75] H. Lessheim and R. Samuel, Curr. Sci. **4**, 584 (1936), https://www.jstor.org/stable/24206071.

[76] E. Perez-Albuerne and H. Drickamer, J. Chem. Phys. **43**, 1381 (1965).

[77] G. Jura and C. W. Garland, J. Am. Chem. Soc. **74**, 6033 (1952).

[78] A. Schleife, F. Fuchs, J. Furthmüller, and F. Bechstedt, Phys. Rev. B **73**, 245212 (2006).

[79] F. Decremps, J. Pellicer-Porres, A. M. Saitta, J.-C. Chervin, and A. Polian, Phys. Rev. B **65**, 092101 (2002).

[80] M. Goano, F. Bertazzi, M. Penna, and E. Bellotti, J. Appl. Phys. **102**, 083709 (2007).

[81] C.-Y. Yeh, Z. W. Lu, S. Froyen, and A. Zunger, Phys. Rev. B **46**, 10086 (1992).

[82] P. Lawaetz, Phys. Rev. B **5**, 4039 (1972).

[83] P. E. Van Camp, V. E. Van Doren, and J. T. Devreese, Phys. Rev. B **44**, 9056 (1991).

[84] P. Denteneer and W. Van Haeringen, Solid State Commun. **65**, 115 (1988).

[85] N. Takeuchi, Phys. Rev. B **65**, 045204 (2002).

[86] Y.-N. Xu and W. Y. Ching, Phys. Rev. B **44**, 7787 (1991).

[87] P. Bhattacharya, R. R. Das, and R. Katiyar, Appl. Phys. Lett. **83**, 2010 (2003).

[88] F. Tian, D. Duan, D. Li, C. Chen, X. Sha, Z. Zhao, B. Liu, and T. Cui, Sci. Rep. **4**, 5759 (2014).

[89] S. Chawla, K. Jayanthi, H. Chander, D. Haranath, S. Halder, and M. Kar, J. Alloys Compd. **459**, 457 (2008).

[90] C. Abed, M. B. Ali, A. Addad, and H. Elhouichet, Mater. Res. Bull. **110**, 230 (2019).

[91] A. Seko, F. Oba, A. Kuwabara, and I. Tanaka, Phys. Rev. B **72**, 024107 (2005).

[92] A. N. Enyashin, I. R. Shein, and A. L. Ivanovskii, Phys. Rev. B **75**, 193408 (2007).

[93] Y.-H. Lin, K. Terai, H. Wadati, M. Kobayashi, M. Takizawa, J. I. Hwang, A. Fujimori, C.-W. Nan, J.-F. Li, S.-I. Fujimori, T. Okane, Y. Saitoh, and K. Kobayashi, Appl. Phys. Lett. **90** (2007).

[94] I. Petousis, D. Mrdjenovich, E. Ballouz, M. Liu, D. Winston, W. Chen, T. Graf, T. D. Schladt, K. A. Persson, and F. B. Prinz, Sci. Data **4**, 1 (2017).

[95] J. M. Munro, K. Latimer, M. K. Horton, S. Dwaraknath, and K. A. Persson, npj Comput. Mater. **6**, 112 (2020).

[96] A. K. Singh, L. Zhou, A. Shinde, S. K. Suram, J. H. Montoya, D. Winston, J. M. Gregoire, and K. A. Persson, Chem. Mater. **29**, 10159 (2017).

[97] A. M. Patel, J. K. Nørskov, K. A. Persson, and J. H. Montoya, Phys. Chem. Chem. Phys. **21**, 25323 (2019).

[98] K. A. Persson, B. Waldwick, P. Lazic, and G. Ceder, Phys. Rev. B **85**, 235438 (2012).

[99] M. K. Horton, J. H. Montoya, M. Liu, and K. A. Persson, npj Comput. Mater. **5**, 64 (2019).

[100] H. Ding, S. S. Dwaraknath, L. Garten, P. Ndione, D. Ginley, and K. A. Persson, ACS Appl. Mater. Interfaces **8**, 13086 (2016).

[101] A. Jain, G. Hautier, S. P. Ong, C. J. Moore, C. C. Fischer, K. A. Persson, and G. Ceder, Phys. Rev. B **84**, 045115 (2011).

[102] A. Wang, R. Kingsbury, M. McDermott, M. Horton, A. Jain, S. P. Ong, S. Dwaraknath, and K. A. Persson, Sci. Rep. **11**, 1 (2021).

[103] M. Aykol, S. S. Dwaraknath, W. Sun, and K. A. Persson, Sci. Adv. **4**, 0148 (2018).

[104] R. Tran, Z. Xu, B. Radhakrishnan, D. Winston, W. Sun, K. A. Persson, and S. P. Ong, Sci. Data **3**, 1 (2016).

[105] M. De Jong, W. Chen, T. Angsten, A. Jain, R. Notestine, A. Gamst, M. Sluiter, C. Krishna Ande, S. Van Der Zwaag, J. J. Plata *et al.*, Sci. Data **2**, 1 (2015).

[106] M. De Jong, W. Chen, H. Geerlings, M. Asta, and K. A. Persson, Sci. Data **2**, 1 (2015).

[107] K. Latimer, S. Dwaraknath, K. Mathew, D. Winston, and K. A. Persson, npj Comput. Mater. **4**, 40 (2018).

[108] H. Zheng, X.-G. Li, R. Tran, C. Chen, M. Horton, D. Winston, K. A. Persson, and S. P. Ong, Acta Mater. **186**, 40 (2020).

[109] C. J. Pickard and R. J. Needs, Phys. Rev. Lett. **97**, 045504 (2006).

[110] A. Wright, Defects in SiO_2 and related dielectrics: science and technology, NATO Science Series II: Mathematics, Physics and Chemistry (Springer Dordrecht, 2000), 10.1007/978-94-010-0944-7.

[111] A. V. Kimmel and A. L. Shluger, J. Non-Cryst. Solids **355**, 1103 (2009).

[112] P. Keating, Phys. Rev. **145**, 637 (1966).

[113] P. Steinmann, A. Smith, E. Birang, A. McBride, and A. Javili, J. Mech. Phys. Solids **154**, 104507 (2021).

[114] S. J. Honrao, S. R. Xie, and R. G. Hennig, J. Appl. Phys. **128** (2020).

[115] See Supplemental Material at http://link.aps.org/supplemental/10.1103/PhysRevLett.132.066201 for further details and discussions (see also Refs. [116–149]). The topics covered include the following: A comparison of RAFFLE with other methodologies, RAFFLE calculation description, *Ab initio* methods, Energies of formation, Accounting for strain effects, Structure schematics.

[116] A. C. T. van Duin, S. Dasgupta, F. Lorant, and W. A. Goddard, J. Phys. Chem. A **105**, 9396 (2001).

[117] M. d'Avezac and A. Zunger, J. Phys. Condens. Matter **19**, 402201 (2007).

[118] G. Trimarchi and A. Zunger, Phys. Rev. B **75**, 104113 (2007).

[119] Q. Wang and L. Zhang, Nat. Commun. **12**, 5359 (2021).

[120] M. Mayo, K. J. Griffith, C. J. Pickard, and A. J. Morris, Chem. Mater. **28,** 2011 (2016).

[121] J. M. Stratford, M. Mayo, P. K. Allan, O. Pecher, O. J. Borkiewicz, K. M. Wiaderek, K. W. Chapman, C. J. Pickard, A. J. Morris, and C. P. Grey, J. Ame. Chem. Soc. **139,** 7273 (2017).

[122] L. E. Marbella, M. L. Evans, M. F. Groh, J. Nelson, K. J. Griffith, A. J. Morris, and C. P. Grey, J. Am. Chem. Soc. **140,** 7994 (2018).

[123] S. Woodley, P. Battle, J. Gale, and C. A. Catlow, Phys. Chem. Chem. Phys. **1,** 2535 (1999).

[124] A. R. Oganov and C. W. Glass, J. Chem. Phys. **124** (2006).

[125] A. L.-S. Chua, N. A. Benedek, L. Chen, M. W. Finnis, and A. P. Sutton, Nat. Mater. **9,** 418 (2010).

[126] K. T. Butler, D. W. Davies, H. Cartwright, O. Isayev, and A. Walsh, Nature (London) **559,** 547 (2018).

[127] T. Wang, C. Zhang, H. Snoussi, and G. Zhang, Adv. Funct. Mater. **30,** 1906041 (2020).

[128] G. Han, Y. Sun, Y. Feng, G. Lin, and N. Lu, ES Mater. Manuf. **14,** 20 (2021).

[129] M. W. Gaultois, A. O. Oliynyk, A. Mar, T. D. Sparks, G. J. Mulholland, and B. Meredig, APL Mater. **4** (2016).

[130] S. Kiyohara, H. Oda, T. Miyata, and T. Mizoguchi, Sci. Adv. **2,** e1600746 (2016).

[131] J. Schmidt, M. R. Marques, S. Botti, and M. A. Marques, npj Comput. Mater. **5,** 83 (2019).

[132] M. Reau, N. Renaud, L. C. Xue, and A. M. Bonvin, Bioinformatics **39,** btac759 (2023).

[133] G. Di Liberto, A. Morales-García, and S. T. Bromley, Nat. Commun. **13,** 6236 (2022).

[134] A. K. Lenstra, H. W. Lenstra, and L. Lovász, Math. Ann. **261,** 515 (1982).

[135] P. K. Sahoo, S. Memaran, Y. Xin, L. Balicas, and H. R. Gutiérrez, Nature (London) **553,** 63 (2018).

[136] H. Aboulfadl, F. Seifried, M. Stüber, and F. Mücklich, Mater. Lett. **236,** 92 (2019).

[137] G. Kresse and J. Hafner, Phys. Rev. B **47,** 558 (1993).

[138] G. Kresse and J. Hafner, Phys. Rev. B **49,** 14251 (1994).

[139] G. Kresse and J. Furthmüller, Comput. Mater. Sci. **6,** 15 (1996).

[140] G. Kresse and J. Furthmüller, Phys. Rev. B **54,** 11169 (1996).

[141] L. He, F. Liu, G. Hautier, M. J. T. Oliveira, M. A. L. Marques, F. D. Vila, J. J. Rehr, G.-M. Rignanese, and A. Zhou, Phys. Rev. B **89,** 064305 (2014).

[142] G.-X. Zhang, A. M. Reilly, A. Tkatchenko, and M. Scheffler, New J. Phys. **20,** 063020 (2018).

[143] J. P. Perdew, K. Burke, and M. Ernzerhof, Phys. Rev. Lett. **77,** 3865 (1996).

[144] P. E. Blöchl, Phys. Rev. B **50,** 17953 (1994).

[145] S. Grimme, J. Antony, S. Ehrlich, and H. Krieg, J. Chem. Phys. **132,** 154104 (2010).

[146] Y. Qi, H. Guo, L. G. Hector, and A. Timmons, J. Electrochem. Soc. **157,** A558 (2010).

[147] J. Tersoff, Phys. Rev. B **39,** 5566 (1989).

[148] R. G. Bell, R. A. Jackson, and C. R. A. Catlow, J. Chem. Soc. Chem. Commun. **31,** 782 (1985).

[149] F. H. Stillinger and T. A. Weber, Phys. Rev. B **31,** 5262 (1985).

[150] N. T. Taylor, F. H. Davies, I. E. M. Rudkin, C. J. Price, T. H. Chan, and S. P. Hepplestone, Comput. Phys. Commun. **257,** 107515 (2020).

[151] D. Hoat, V. Van On, D. K. Nguyen, M. Naseri, R. Ponce-Pérez, T. V. Vu, J. Rivas-Silva, N. N. Hieu, and G. H. Cocoletzi, RSC Adv. **10,** 40411 (2020).

[152] A. Wander, I. J. Bush, and N. M. Harrison, Phys. Rev. B **68,** 233405 (2003).

[153] B. E. Gaddy, E. A. Paisley, J.-P. Maria, and D. L. Irving, Phys. Rev. B **90,** 125403 (2014).

[154] J. Pitfield, N. T. Taylor, and S. P. Hepplestone, Predicting phase stability at interfaces (dataset), 10.24378/exe.4966.

[155] https://www.archer2.ac.uk/.